Spin-wave modes and line broadening in strongly coupled epitaxial Fe/Al/Fe and Fe/Si/Fe trilayers observed by Brillouin light scattering

B. K. Kuanr,[a)] M. Buchmeier, R. R. Gareev, D. E. Bürgler, R. Schreiber, and P. Grünberg

Institut für Festkörperforschung, Forschungszentrum Jülich GmbH, D-52425 Jülich, Germany

We report on the spin-wave excitation frequencies and the broadening of the mode linewidths in Stokes and anti-Stokes Brillouin light scattering spectra of strongly exchange coupled (2–6.5 mJ/m^2), epitaxial trilayers with the following structures: Fe(80 Å)/Si wedge/Fe(100 Å) and Fe(50 Å)/Al wedge/Fe(70 Å). Both spacer materials yield qualitatively similar spectra which evolve in the same way when the spacer thickness increases. We determine the type of interlayer coupling and quantify its strength as a function of the spacer thickness by comparing and fitting the mode positions to a model calculation. Furthermore, we observe clearly different behaviors of the mode linewidths as a function of spacer thickness for the optic and acoustic modes. There are also strong differences between the Stokes and anti-Stokes side of the spectra. The largest linewidths of up to 8 GHz occur at spacer thicknesses between 5 and 8 Å for both spacer materials. Lateral averaging and two-magnon scattering are qualitatively discussed as possible sources for the line-broadening. © *2003 American Institute of Physics.* [DOI: 10.1063/1.1554758]

I. INTRODUCTION

Brillouin light scattering (BLS) is a powerful, nonde-structive dynamic technique to investigate the fundamental parameters of magnetic thin films and multilayers by studying electromagnetic radiation inelastically scattered by thermal spin waves (magnons). So far most BLS studies on magnetic trilayers and multilayers with interlayer coupling have been performed with spacers like Cu, Ag, and Cr which yield interlayer exchange coupling of the order of 1 mJ/m^2.[1–10] Antiferromagnetic (AF) interlayer exchange coupling leading to antialignment of the film magnetizations can directly be identified from a BLS spectra because—under certain geometric conditions given below—antialignment leads to an asymmetry of the mode positions on the Stokes (magnon creation) and anti-Stokes (magnon annihilation) side of the spectra.[1,11] The strength of the coupling can be obtained from fitting the mode positions to a model calculation for both ferromagnetic (FM) and AF coupling without the need to remagnetize and saturate the sample in an external field.

Here we present a comprehensive BLS study of two strongly AF exchange coupled (>2 mJ/m^2) trilayer systems, namely Fe/Si/Fe and Fe/Al/Fe first described in Refs. 12 and 13, respectively. We quantitatively evaluate the mode positions to determine the coupling strength. Using a new type of model calculation we explicitly take into account nonuniform magnetization structures in the FM films that arise due to strong AF interlayer coupling. Moreover, we observe the influence of the interlayer coupling on the magnon linewidths and discuss possible mechanisms for the observed linebroadening.

II. EXPERIMENT

Brillouin light scattering experiments are performed at room temperature (RT) utilizing *p*-polarized laser light with a wavelength of λ = 532 nm incident at an angle $\alpha = 45°$. The laser power is less than 60 mW to avoid undesirable sample heating. The *s*-polarized backscattered light is collected by a camera lens ($f = 1.4$) and analyzed with a (2×3) pass Tandem Fabry–Pérot interferometer.[1] In this geometry the magnon wave vector becomes $q = 4\pi/\lambda \sin(\alpha) = 1.67 \times 10^7$ m^{-1}. The external magnetic field is applied in the film plane and normal to the scattering plane of the laser light. The cross polarization geometry prevents phonon lines in the spectra. We use an avalanche diode detector and an Oxford MCS-II card connected to a PC for data acquisition.

The surface modes of the acoustic and optic spin-waves are recorded on both the Stokes and the anti-Stokes side of the elastic peak. The magnetic film thicknesses are chosen thin enough so that the higher order exchange modes are shifted well outside the free spectral range of 45 GHz used for the present investigation. The diameter of laser spot is about 40 μm and thus small enough compared to the slope of the wedges (0.7–1.4 Å/mm) to allow precise measurements of coupling strength along the wedge, as confirmed by control measurements with flat spacers, i.e., with vanishing wedge slopes.

Epitaxial wedge-type Fe(80 Å)/Si(0–22 Å)/Fe(100 Å) and Fe(50 Å)/Al(0–11 Å or 0–20 Å)/Fe(70 Å) trilayers are grown by thermal *e*-gun evaporation in an ultrahigh vacuum (UHV) system with a background pressure better than 10^{-10} mbar. A 150-nm-thick Ag(001) buffer layer is first grown on UHV-annealed GaAs(001) substrates according to the recipe used in Refs. 14 and 15. In order to minimize segregation of Ag the first 4 ML of the bottom Fe layers are grown at RT and the remaining at 200–250 °C. The growth temperature for the interlayer are RT in the case of Si and 80 °C for Al.

The top Fe layer and a ZnS cover layer are grown at RT. All deposition rates are controlled by calibrated quartz-crystal monitors. *In situ* characterization is performed with Auger electron spectroscopy (AES), low energy electron diffraction (LEED), and reflection high energy electron diffraction (RHEED). AES spectra and well defined RHEED and LEED diffraction patterns of all layers indicate epitaxial growth throughout both systems.

III. COUPLED SPIN-WAVE MODES

In a BLS experiment the frequency of spin-waves (magnons) ν is measured via inelastic scattering of monochromatic light. The frequency of the scattered photons can be shifted either down or up by ν corresponding to the creation (Stokes condition) or annihilation (anti-Stokes condition) of a magnon, respectively. As the in-plane momentum is conserved, the in-plane wave vector of the probed magnons q is well defined by the scattering geometry.

In analogy to coupled harmonic oscillators (e.g., phonons), the magnon modes in two magnetic films coupled via a non-magnetic interlayer can be classified into acoustic (A) and optic (O) modes depending on whether the two film magnetizations precess in-phase or 180°-out-of-phase, respectively. This assignment is straightforward when the film magnetizations are in parallel (P) alignment. For the antiparallel (AP) alignment the two magnetizations precess in opposite directions, and hence their relative phase changes continuously. However, the precessional motions are strongly elliptical because the thin film geometry gives rise to strong shape anisotropy, which forces the magnetization into the film plane. The long axis of these precessional ellipses lie in the film plane. Considering only the dominant in-plane component of the dynamic magnetization which performs a pendulum motion it is possible to distinguish in-phase, acoustic and out-of-phase, optic modes.

The frequency of the optic spin-wave modes strongly depends on the interaction, i.e., the interlayer coupling, whereas the acoustic spin-wave modes are almost independent of the coupling strength, again in analogy to coupled harmonic oscillators. However, the acoustic mode frequency depends on the alignment (AP or P) of the film magnetizations. Dipolar interaction between the dynamic magnetizations leads to a lower mode frequency for the AP alignment. Hence, the mode frequency of the acoustic mode can solely be used to determine the AF coupling strength via the switching from AP to P alignment, similar to the situation for remagnetization measurements as for instance in a magneto-optical Kerr effect (MOKE) experiment. In contrast, the optic mode allows a determination of the sign and strength of the interlayer coupling without applying a saturating field: With increasing AF coupling strength the optic mode frequency shifts up for AP alignment and down for P alignment because the AF coupling represents a restoring force for the AP but not for the P alignment. For FM coupling the behavior is the opposite: The optic mode frequency shifts up for P alignment and down for AP alignment.

When the static parts of the magnetizations have components perpendicular to the magnon wave vector q and oppo-
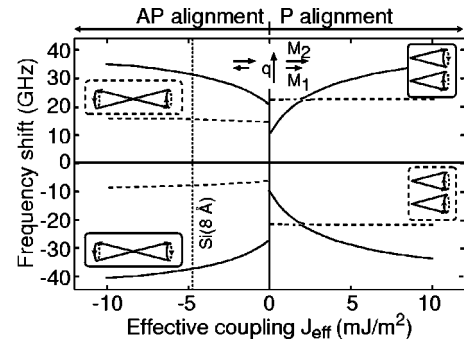

FIG. 1. Calculated acoustic (dashed line) and optic (solid line) spin-wave frequencies of a Fe(001)(80 Å)/spacer/Fe(100 Å) system in zero field as a function of effective coupling J_{eff} defined in Eqs. (3) and (4). Insets show the precession directions of the magnetizations. The dominant in-plane components lie in the plane of the drawing and perform in-phase or out-of-phase pendulum motions. The dotted, vertical line indicates J_{eff} for a 8-Å-thick Si spacer and yields mode frequencies in good agreement with spectrum (f) in the right part of Fig. 2.

site in direction, then the dipolar interaction gives rise to the Stokes anti-Stokes asymmetry for AP alignment. For P alignment such an asymmetry never does occur (Fig. 1). In order to make sure that the above condition is fulfilled we use two different ferromagnetic (Fe) layer thicknesses. Even for AP alignment this results in a non-zero net magnetization which aligns the film magnetizations P and AP, respectively, to the external field which we apply perpendicular to magnon wave vector q defined by the scattering plane of the light (Voigt geometry).

Measuring at a fixed external magnetic field allows us to study the magnetic excitations when the film magnetizations are in P, AP, or in a canted alignment at different spacer thicknesses, i.e., for different coupling conditions. The coupling is parameterized by the bilinear (J_1) and biquadratic (J_2) coupling parameters defined via the phenomenological energy density expression

$$E_J = -J_1\cos(\Delta\theta) - J_2\cos^2(\Delta\theta), \tag{1}$$

where $\Delta\theta$ is the angle between the static film magnetizations.

IV. MODEL CALCULATION

The main goal of a model calculation is to calculate the mode positions as a function of the coupling strengths such that we can derive the coupling parameters as a function of spacer thickness. Previously, BLS spectra were calculated based on the model described in Refs. 8 and 16. This model assumes thin ferromagnetic layers and weak coupling such that a single domain state with homogeneous magnetization can be considered. Furthermore, the (bilinear and biquadratic) interlayer exchange is treated as a volume effect. In fact, however, this interaction only applies a torque to the moments at the interfaces which is then transferred by direct exchange coupling to neighboring layers into the bulk of the ferromagnetic material. Thus, a partial domain wall parallel to the interface may form due to competitive torques exerted at the interface by the coupling and in the bulk by the external field.[17] Furthermore, strong coupling gives rise to non-

uniform mode profiles with nodes or peaks at the interface depending on the alignment of the film magnetizations and the sign of the coupling.[18,19] For strong coupling the critical thickness where these effects become significant decreases. For these reasons the standard ultrathin film approximation used to calculate BLS spectra,[8,16] which assumes both homogeneous static magnetizations and uniform spin-wave mode profiles perpendicular to the layers, cannot be applied to our samples with too strong coupling.

We use an extended method to calculate the spin-wave frequencies. We virtually divide the ferromagnetic layers into n thin sublayers with in-plane magnetization angles θ_i ($i = 1 \ldots n$). The intralayer exchange energy density can be written as an effective interlayer coupling between the sublayers

$$E_{\mathrm{ex}} = -\sum_{i=1}^{n-1} 2A \frac{n}{d} \cos(\theta_i - \theta_{i+1}), \tag{2}$$

where A is the exchange constant and d the thickness of the ferromagnetic film. This form holds for small sublayer-to-sublayer increments of the angle ($|\theta_i - \theta_{i+1}| \ll 1$) which can be achieved by an appropriate choice of n. This expression has the same form as the bilinear interlayer coupling in a multilayer. Thus, the ultrathin film approximation generalized for a multilayer system can readily be used to calculate the spin-wave frequencies. The formation of a twisted static magnetization structure is taken into account by computing the minima of the total free energy of the virtual multilayer as a function of the in-plane magnetization angles θ_i. The twisted state appears due to a torque of the external field. Therefore, the inclusion of the twisted state is of importance for the correct description of field dependent experiments. The determination of coupling constants under the assumption of uniform static and dynamic magnetizations leads to systematic errors, in particular J_2 is overestimated by about a factor 3 in regions with strong coupling. In cases with very strong coupling and/or thicker FM layers, satisfactory fits without considering nonuniform magnetizations are not at all possible. Details of the model and calculation procedures will be published elsewhere.[20]

The total free energy is composed of the Zeeman energy of each sublayer due to the external field, the fourfold cubic anisotropy, intralayer exchange [Eq. (2)], the interlayer exchange with bilinear and biquadratic contributions according to Eq. (1), and the dipolar energy. Dipolar contributions arise from to the shape anisotropy forcing the magnetizations into the plane of the sample and from the dynamic dipolar coupling of the layers that is treated in the lowest order of single-layer magnon modes.[16]

Figure 1 depicts the calculated mode positions of the optic and acoustic modes in P and AP alignment at zero external field *versus* the effective coupling strength J_{eff} defined as

$$J_{\mathrm{eff}} = J_1 + 2J_2 \tag{3}$$

for P alignment, and

$$J_{\mathrm{eff}} = J_1 - 2J_2 \tag{4}$$

for AP alignment. In zero field the sign of J_{eff} determines the alignment of the magnetizations. For nonzero fields this is not necessarily the case, e.g., at fields larger than the saturation field the films are always in P alignment, even for AF coupling. Thus, it is important to carefully distinguish between the magnetization alignment at a certain field and the type (FM, AFM, or 90°) of the coupling. We assume Fe layers of 80 and 100 Å thickness with a 10-Å-thick interlayer and use the following parameters: Saturation magnetization of Fe $M_S = 1.65 \times 10^6$ A/m, four-fold anisotropy constant $K_1 = 45$ kJ/m^3, gyromagnetic ratio $\gamma/2\pi = 29.4$ GHz/T ($g = 2.1$), exchange constant $A = 2 \times 10^{11}$ J/m, and $q = 1.67 \times 10^7$ m^{-1}. The insets show the precession of the magnetizations. The in-plane components lie in the plane of the drawing and perform an in-phase or out-of-phase pendulum motion. Based on these motions we denote the modes acoustic and optic, respectively (see Sec. III). At external fields much lower than the saturation field and for $|J_1| > |2J_2|$ both film magnetizations M_1 and M_2 align either parallel to the external field for P alignment (right side) or antiparallel to each other with the larger magnetization M_2 in field direction for AP alignment (left side). For $|J_1| < |2J_2|$ and $J_2 < 0$ the film magnetizations are in a canted state, and Fig. 1 cannot be applied for the interpretation of experimental spectra. The acoustic mode only shows a jump when the alignment of M_1 and M_2 changes, whereas the optic modes additionally strongly depend on the magnitude of J_{eff} as discussed in Sec. III. For P alignment the optic mode can have a lower or a higher frequency than the acoustic mode depending on the value of J_{eff}. A separation of J_1 and J_2 is only possible in special cases, for example for clear noncollinear alignment. However, the separation is readily feasible using the field dependence of the BLS mode positions as has been done in Refs. 12 and 13 for Fe/Si/Fe and Fe/Al/Fe, respectively. An example for the field dependence of BLS spectra will be given in Sec. VI for a Fe(80 Å)/Al(12 Å)/Fe(130 Å) sample. For most of the spectra presented in Sec. V, P or AP alignment can be directly determined from the position of the acoustic mode. Only few spectra show a canted alignment.

Figure 1 also shows the asymmetry between the Stokes and anti-Stokes side of the spectra for AP alignment. It arises from dipolar interactions and has first been observed and identified as an indicator for AP alignment by Grünberg *et al.*[1]

V. LINE POSITIONS

BLS spectra including both the Stokes and the anti-Stokes sides for different spacer thicknesses are presented in Fig. 2 for both types of wedge-type trilayers, Fe/Al/Fe (left) and Fe/Si/Fe (right). Acoustic modes identified by their higher intensity and by comparison with the model calculations discussed in Sec. IV are gray colored. A small external field (compared to the saturation field) of 30 mT was applied during the measurement in order to obtain the desired magnetic alignment specified in Sec. III. This field is kept constant such that we can exclude different external fields as a source of the linewidth variations presented in Sec. VI. The evolution of the spectra with spacer thickness for the two
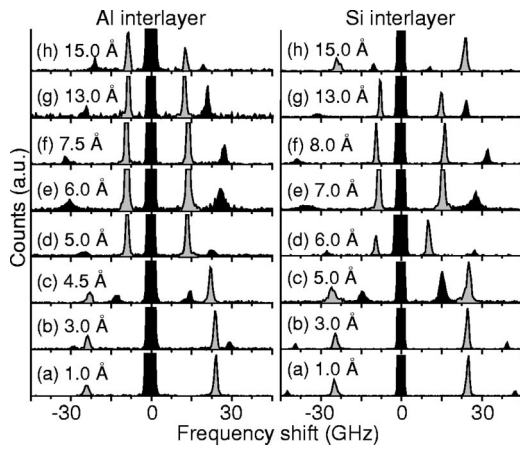
FIG. 2. Examples of BLS spectra taken at different interlayer thicknesses t along wedge-type Fe(50 Å)/Al wedge/Fe(70 Å) (left part) and Fe(80 Å)/Si wedge/Fe(100 Å) (right part) samples. An external field of 30 mT is applied along a [100] easy axis of Fe. Gray colored peaks are assigned to acoustic modes.
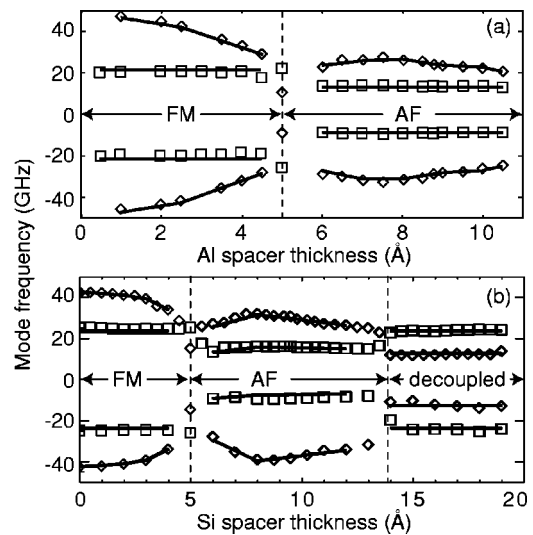
FIG. 3. Mode frequencies for wedge-type Fe(50 Å)/Al wedge/Fe(70 Å) (a) and Fe(80 Å)/Si wedge/Fe(100 Å) (b) trilayers as a function of the interlayer thicknesses. An external field of 30 mT is applied along a [100] easy axis of Fe. Squares ($\square$) represent acoustic modes and diamonds ($\diamond$) optic modes. Solid lines are fits based on the model calculation using the parameters given in Sec. IV. Regions with different dominant coupling types are labeled and indicated by dashed lines.

systems is qualitatively very similar and can be discussed together. The comparison with Fig. 1 immediately allows a qualitative interpretation.

For very thin interlayers of 1 Å thickness the optic peak is observed at much higher frequency than the acoustic peak [spectra (a), the optic peaks of the Fe/Al/Fe system are outside the frequency range], and the Stokes and anti-Stokes sides are symmetric. Therefore, the film magnetizations are in P alignment, which is the result of strong FM coupling. Direct exchange of the two magnetic layers giving rise to FM coupling must be expected at this very small spacer thickness, although pinholes are another possible reason too. With the increase of the interlayer thickness to 3 Å [spectra (b)] the acoustic modes remain unchanged, whereas the optic mode comes down in frequency indicating a decrease of FM coupling strength. At this spacer thickness direct exchange becomes small, and the still rather strong FM coupling could be attributed to pinholes whose number decreases with spacer thickness. The next spectra (c) show a shift of the optic mode to a lower frequency than the acoustic mode. This is due to a further, sharp decrease of the FM coupling strength and corresponds to P alignment with a small, positive effective coupling J_{eff} (see Fig. 1). For Al there appears a weak Stokes anti-Stokes asymmetry which contradicts the P alignment. Therefore, a canted alignment is the most likely interpretation of the Al spectrum (c). In spectra (d) at t_{Al} $= 5$ Å and $t_{Si} = 6$ Å there is an abrupt jump of the acoustic mode frequency to a much lower value. This jump reflects the transition of the magnetization alignment from P to AP. Additionally, the peak separation on the Stokes and anti-Stokes side becomes different and thus asymmetric as expected for AP or canted alignment of the magnetizations. Therefore, at $t_{Al} = 5$ Å and $t_{Si} = 6$ Å FM coupling is overcome by AF or 90° interlayer coupling. In spectra (e) the Stokes anti-Stokes asymmetry further increases to become maximal in spectra (f) for $t_{Al} = 7.5$ Å and $t_{Si} = 8$ Å. In these regions the AF coupling is dominant and the magnetizations are AP aligned. The vertical, dotted line in Fig. 1 yields, as an example, the mode frequencies for the Si spectrum (f) at

$t_{Si} = 8$ Å: -39, -10, 16, and 32 GHz. The increase of interlayer thickness to 13 Å [spectra (g)] leads for both systems to a drop of the optic mode frequency accompanied by a reduction of the Stokes anti-Stokes asymmetry. At the largest interlayer thickness of 15 Å shown in spectra (h) we observe a distinct material related difference: In the case of Si there is a interchange of optic and acoustic mode positions such that the optic mode lies below the acoustic. As can be seen in Fig. 1, this situation may occur for P alignment and weak FM coupling or for the decoupled state ($J_{eff} = 0$ in Fig. 1). In the case of Al, however, there is no interchange of the mode positions, and there still exists a weak Stokes anti-Stokes asymmetry. Thus, for the Al interlayer the AF coupling has a long tail to rather large spacer thicknesses.

In Fig. 3 we plot the mode frequencies of both the Stokes and anti-Stokes sides measured in an external field of 30 mT applied along Fe[100] easy axis for a Fe(50 Å)/Al wedge)/Fe(70 Å) trilayer and a Fe(80 Å)/Si wedge)/Fe(100 Å) trilayer. Note that these data originate partly from samples other than the spectra in Fig. 2. The solid lines are fits to the data which allow the determination of the coupling type and strength. The Fe/Al/Fe system shows FM coupling up to an Al thickness of about $t_{Al} \approx 5$ Å and AF coupling for larger thicknesses in agreement with Fig. 2, where we observe AF coupling even for $t_{Al} = 15$ Å. In contrast, the Fe/Si/Fe system exhibits three different coupling regions, FM for small thicknesses up to $t_{Si} \approx 5$ Å, dominating AF coupling for 5 Å$< t_{Si} < 14$ Å, and a very weakly FM coupled or decoupled part for $t_{Si} > 14$ Å. A very narrow region of canted alignment appears for both sample types at the transition from FM to AF coupling at about 5 Å. The fits of the spectra yield a clearly higher effective coupling J_{eff} for the Fe/Si/Fe trilayers compared to the Fe/Al/Fe system. In Figs. 4(a) and 5(a) we plot the fitted J_{eff} as stars for all thicknesses where
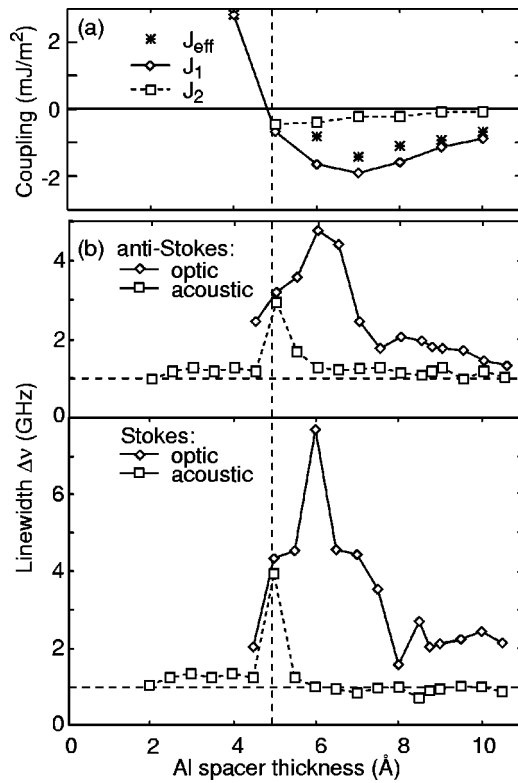
FIG. 4. Coupling constants J_{eff}, J_1, and J_2 (a) and linewidth $\Delta\nu$ (b) of a wedge-type Fe(50 Å)/Al wedge/Fe(70 Å) trilayer vs interlayer thickness. Horizontal dashed lines in (b) indicate the instrumental linewidth limit. The vertical dashed line corresponds to the FM to AF coupling transition of Fig. 3(a).

FIG. 5. Coupling constants J_{eff}, J_1, and J_2 (a) and linewidth $\Delta\nu$ (b) of a wedge-type Fe(80 Å)/Si wedge/Fe(100 Å) trilayer vs interlayer thickness. Horizontal dashed lines in (b) indicate the instrumental linewidth limit. The vertical dashed lines correspond to the coupling regions of Fig. 3(b).

the alignment is either *P* or *AP*. Additionally, we plot the thickness dependence of J_1 and J_2 that we have obtained from fitting the field dependent BLS spectra of Refs. 12 and 13 with our extended model calculation. Using Eqs. (3) and (4) we find good agreement between J_{eff} and the corresponding J_1 and J_2 values.

The FM coupling strength at smallest thicknesses exceeds +6 mJ/m^2 for both systems and then decreases rapidly and passes through zero at about 5 Å. An AF peak develops for both sample types at 7 Å with maxima of $J_1 \approx -2$ mJ/m^2 for Al and $J_1 \approx -6.5$ mJ/m^2 for Si. The onset of AF coupling is accompanied by biquadratic coupling J_2 which gives rise to a canted alignment in the transition regions where $J_1 \approx J_2$. J_2 always remains smaller than J_1 ($|J_2| < 0.5$ mJ/m^2 for Al and $|J_2| < 3$ mJ/m^2 for Si), and J_2 also decays quicker than J_1. This confirms our interpretation of the spectra that there is only a narrow thickness range with canted alignment of the film magnetizations.

The AF coupling across Al decays rather slowly as previously reported in Ref. 13. This behavior is still unclear and could be due the fact that for Al the Fermi wave vector k_F almost reaches the boundary of the first Brillouin zone ($K/2$). Therefore, the caliper $k_C = |2k_F - K|$ is small and the resulting oscillation period[21,22] $\lambda = 2\pi/k_C$ is big such that the second oscillation maximum occurs at a large spacer thickness beyond the thickness range studied here. Another explanation could be a Stranski–Krastanov-type growth mode for Al on Fe. Due to the initial wetting of the Fe substrate the
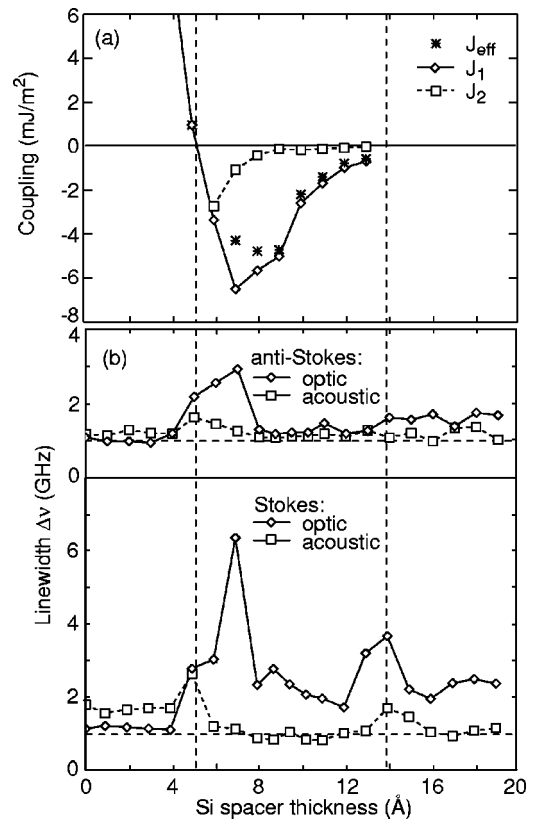
FM coupling is efficiently suppressed and the coupling becomes AF for small Al thickness. The subsequent three-dimensional (3D) growth then leads to the slow decay of the AF coupling because the "valleys" between the growth hillocks mediate relatively strong AF coupling even for large nominal Al spacer thicknesses. This mechanism also suppresses possibly present intrinsic oscillations of the coupling.

The coupling in Fe/Si/Fe decays quickly and becomes small for $t_{\text{Si}} \gtrsim 14$ Å in agreement with the results in Ref. 12 derived from MOKE loops and field dependent BLS. In particular, there is no oscillatory component of the coupling. In this case the absence of oscillations is related to the high resistivity of the nominally pure Si spacer.[12,23]

VI. MODE LINEWIDTHS

In addition to the variation of mode frequencies ν, the linewidths ($\Delta\nu$) measured as the full width at half maximum are observed to vary along the wedges in a dramatic manner [Figs. 4(b) and 5(b)]. The two types of samples show qualitatively similar behavior and will be discussed together. A first inspection of the data reveals that the linewidths for the acoustic and optic modes as well as for the Stokes and anti-Stokes sides behave significantly differently.

The linewidth of the optic mode is larger (up to almost 8 GHz) than for the acoustic mode except for the FM coupled region at spacer thicknesses smaller than 5 Å, where both the linewidth of the optic mode ($\Delta\nu_O$) and the linewidth of the
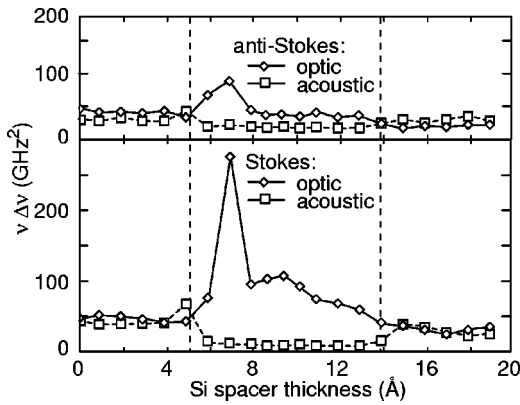
FIG. 6. Frequency times linewidth $\nu\Delta\nu$ of a wedge-type Fe(50 Å)/Si wedge/Fe(70 Å) trilayer vs interlayer thicknesses. Vertical dashed lines correspond to the coupling regions of Fig. 3(b).
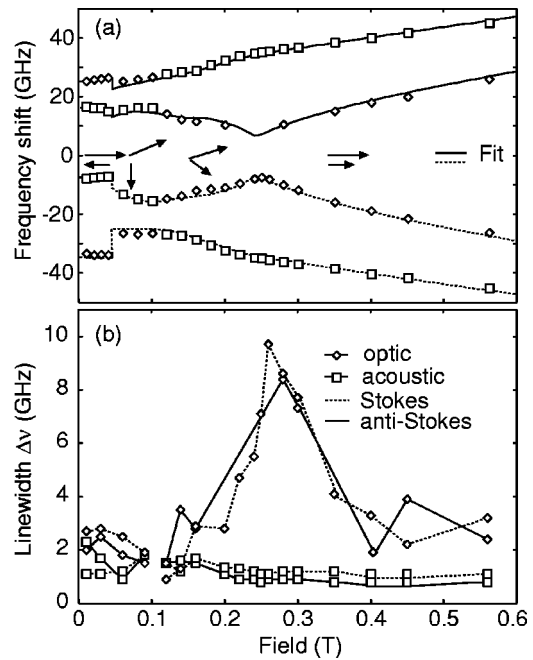

FIG. 7. (a) Field dependence of the mode frequencies for a Fe(80 Å)/Al(12 Å)/Fe(130 Å) sample. The external field is applied in the film plane and normal to the scattering plane of the laser light. Solid and dotted lines are fits according to our model calculation. (b) Field dependence of the mode linewidth. Lines are guides to the eyes.

acoustic mode $(\Delta\nu_A)$ drop to the instrumental resolution limit of about 1 GHz. In the case of Si the acoustic linewidth in this region is slightly larger. Both linewidths become clearly larger at the onset of biquadratic coupling and AP alignment (5 Å). $\Delta\nu_O$ remains larger for the whole AF coupled region with a distinct maximum at $t_{Al}=6$ Å or $t_{Si}=7$ Å, respectively. In contrast, $\Delta\nu_A$ shows peaks exactly in the region of canted alignment at the transition from P to AP and then quickly drops to the instrumental linewidth. All linewidths are larger and all effects are much more pronounced on the Stokes side of the spectra. The direct comparison with the coupling parameters in Figs. 4(a) and 5(a) does not show a direct correlation between $\Delta\nu$ and J_1 or J_2 neither for the acoustic nor the optic branch. There is also no simple scaling between mode frequencies ν and linewidths $\Delta\nu$. For instance, the maximum of ν_O always occurs at larger spacer thicknesses than the peak in $\Delta\nu_O$.

Similar conclusions can be drawn for the behavior of the quantity $\nu\Delta\nu$ plotted in Fig. 6 for the Si case. If we plot $\nu\Delta\nu$ for the Al sample we obtain qualitatively similar curves. The maximum of $\nu_O\Delta\nu_O$ coincides with the coupling maximum, but the peak shapes are clearly different. The quantities $\nu\Delta\nu$ show a direct correlation to the alignment: $\nu_O\Delta\nu_O$ and $\nu_A\Delta\nu_A$ are equal for P alignment. For AP alignment $\nu_A\Delta\nu_A$ is slightly lower and constant, whereas $\nu_O\Delta\nu_O$ is larger and shows a pronounced peak. Again, these effects are much stronger on the Stokes side of the spectra.

We have additionally examined the field dependence of the linewidth as shown in Fig. 7 for a Fe(80 Å)/Al(12 Å)/Fe(130 Å) sample. Open symbols in Fig. 7(a) are the experimental mode frequencies shown together with the excellent fit to our model (solid and dotted lines). Pairs of arrows indicate the magnetization alignment which passes through the following states: AP aligned with the external field, canted, and saturated. The spin–flop transition between AP and canted at about 50 mT and saturation at about 250 mT can clearly be recognized by discontinuities of both modes and a dip of the optic mode, respectively. The fit yields the coupling constants $J_1=-1.1$ mJ/m^2 and $J_2=-0.3$ mJ/m^2. There is a strong increase of $\Delta\nu_O$ in the region of saturation with maximum values of almost 10 GHz, but no strong dependence on the external field and the

magnetization alignment in all other parts of the curve. $\Delta\nu_A$ is rather constant for all fields and insensitive to the alignment, even at the spin–flop transition where the magnetization directions change abruptly.

We can exclude direct damping of the spinwaves due to structural interface roughness as the dominant source for the line broadening because interface roughness gradually changes along the wedge. Furthermore, it should have an equal effect on acoustic and optic modes. Similar arguments apply for the scattering from additional spin wave modes associated with geometrical defects suggested in Ref. 24.

Another possibility for the line broadening is scattering from dipolar stray fields of defects. However, we expect this contribution to depend on the magnetization alignment, and thus we can exclude it as a main origin of line broadening because the linewidths are found in Fig. 7 to be largely independent of the alignment. Furthermore, the interlayer thicknesses considered here are much smaller than the decay length of the dipolar interaction (given by q), such that this effect should not vary as a function of spacer thickness. But we observe strong variations with the spacer thickness in Figs. 4(b) and 5(b).

A more likely reason for the broadening is magnetic inhomogeneities giving rise to nonuniform local coupling. Of course, these can arise from structural inhomogeneities, e.g., thickness fluctuations of the spacer layer. First we estimate the line broadening due to the wedge shape of the interlayer which results in a variation Δt of the spacer thickness within the laser spot of diameter Δl. The variation $\Delta\nu_{wedge}$ over which the laser spot averages is given by

$$\Delta \nu_{\text{wedge}} = \frac{\partial \nu}{\partial t} \Delta t = \frac{\partial \nu}{\partial t} w \Delta l, \tag{5}$$

where w is the wedge slope. Estimating $\partial \nu / \partial t < 5$ GHz/Å from Fig. 3 and using $\Delta l = 40$ μm and $w = 1.4$ Å/mm, we obtain $\Delta \nu_{\text{wedge}} < 0.3$ GHz, which is about 1 order of magnitude smaller than the actually observed linewidths. This is in agreement with the fact that we observe similar linewidths for different samples with wedge slopes in the range from 0.7 to 1.4 Å/mm and also for control samples with flat spacers, i.e., $w = 0$ [compare Fig. 4(b) for $t_{\text{Al}} = 12$ Å with Fig. 7(b) at 30 mT].

Next we consider variations of the local coupling yielding different mode frequencies which are then averaged within the laser spot. Since the optic mode is sensitive to the coupling strength, whereas the acoustic mode is only indirectly sensitive to the coupling via the magnetization alignment, this mechanism could explain the different behavior of $\Delta \nu_O$ and $\Delta \nu_A$. If the coupling variations (e.g., due to thickness fluctuations) occur on a small lateral length scale, then they can give rise to biquadratic coupling.[25] In this case the linewidth should be correlated to J_2. For larger lateral length scales we proceed similarly to Eq. (5) and estimate the variation of the mode frequency due to interface roughness σ

$$\Delta \nu_J = \frac{\partial \nu}{\partial J} \Delta J = \frac{\partial \nu}{\partial J} \frac{\partial J}{\partial t} \sigma. \tag{6}$$

The roughness σ is a smooth function of the spacer thickness t and cannot account for the observed peaks. The acoustic mode is not sensitive to the coupling strength, hence $\partial \nu / \partial J$ is vanishing except for the thicknesses where J_{eff} changes sign, i.e., where the magnetization alignment changes (Fig. 1). There, ν_A jumps abruptly. Therefore, the peaks of $\Delta \nu_A$ at the transition from P to AP or canted and vice versa [e.g., Fig. 5(b)] are compatible with this mechanism.

For the optic branch the situation is less clear. Here, $\partial \nu / \partial J$ does not vanish but it is a rather smooth function of t with an increase for small J_{eff} (Fig. 1). However, the linewidths are not enhanced for small coupling. Therefore, $\partial J / \partial t$ is the dominant factor in Eq. (6), and indeed, it can account for peaks of $\Delta \nu_O$ at spacer thicknesses of 6–7 Å, where $J(t)$ sharply decreases, but the similarly steep increase of $J(t)$ [e.g., Fig. 5(a)] after the coupling maximum does not show up in $\Delta \nu_O$. Thus, the averaging mechanism [Eq. (6)] can explain some but not all features of the linewidths behavior.

We now turn to another mechanism for line broadening, namely two-magnon scattering proposed by Arias and Mills[26] and recently applied to exchange-bias systems by Rezende *et al.*[27] A regular array of pits was assumed at the ferromagnet/antiferromagnet interface that gives rise to a spatially varying direct exchange interaction. The linewidth $\Delta \nu_{\text{scattering}}$ due to two-magnon scattering at the fluctuating local exchange field could be written as[27]

$$\Delta \nu_{\text{scattering}} \propto \frac{H_I^2}{\nu}, \tag{7}$$

where H_I is a measure of the local perturbation of the exchange field. The parameters describing the geometry of the interface enter the proportionality factor together with material constants. In our case, two-magnon scattering occurs at interfaces between the magnetic layers and the spacer where variations of the coupling strength act as scattering potentials. Assuming a similar functional dependence we write the linewidth as

$$\Delta \nu_{\text{scattering}} \propto \frac{\Delta H_{\text{ex}}^2}{\nu}, \tag{8}$$

where ΔH_{ex} is a measure of the local perturbation of the average exchange field, $J_{\text{eff}} / M_S d$. d is the thickness of the magnetic layer. The appearance of ν in the denominator of Eq. (7) is shown by Rezende *et al.*[27] to arise from the strength of the scattering potential. As we deal with a similar origin of the scattering potential—fluctuations of the exchange field due to variation of the interlayer exchange coupling strength in our case and due to variations of the interface exchange coupling in their case— we can assume that the linewidth is inversely proportional to ν. Thus, $\nu \Delta \nu$ is a measure of the "two-magnon scattering strength." This is why we plot this quantity in Fig. 6 for the Fe/Si/Fe structure. As mentioned above, the corresponding curve for Al spacers looks qualitatively similar. The clear correlation of $\nu_O \Delta \nu_O$ with the presence of AP alignment supports the two-magnon scattering mechanism. At the transition from P to AP alignment there is a pronounced competition between strong FM coupling probably across pinholes and strong AF coupling across the interlayers. Therefore, ΔH_{ex} becomes large and gives rise to the peak in $\Delta \nu_O$. At the second transition from AP to P alignment there are also competing couplings but their strengths are much weaker, and hence the fluctuations ΔH_{ex} are smaller. The two-magnon scattering mechanism leads to Lorentzian line shapes, whereas the averaging mechanisms [Eqs. (5) and (6)] are expected to produce Gaussian line shapes. Unfortunately, the statistics of the spectra do not allow a definite statement about the peak shape. Most likely, the peaks must be described by mixture of Gaussian and Lorentzian curves, indicating that both the averaging and the scattering mechanism are operative.

From these qualitative considerations we find that both lateral averaging [Eq. (6)] and two-magnon scattering [Eq. (8)] show up as features of the linewidth curves. However, neither of them can account for all observed features or explain the strongly different linewidths on the Stokes and anti-Stokes sides of the spectra. Qualitatively, the linewidths, in particular $\Delta \nu_O$, are rather sensitive to magnetic inhomogeneities arising: (i) from competing couplings as in the transitions regions and (ii) from fluctuations of the interlayer coupling, in particular in the region of AP alignment, which both give rise to fluctuations of the magnetization directions. Directional fluctuations are also a likely origin of the strongly enhanced optical linewidths near saturation in Fig. 7.

VII. CONCLUSIONS

We present BLS spectra of magnetic trilayer structures with strong AF interlayer exchange coupling. The line positions of the BLS spectra (Stokes and anti-Stokes side) are well understood and are successfully calculated using an ex-

tended model calculation that is especially suited for strong interlayer coupling. The variation of the line position along the wedge-shaped spacer of the trilayers is interpreted in terms of different coupling regimes, and the coupling strengths are quantitatively derived from the spectra.

The linewidths of the modes as a function of the spacer thickness— and hence the coupling—show a rich structure with significant differences between Stokes and anti-Stokes sides as well as between acoustic and optic modes. Lateral averaging and two-magnon scattering are qualitatively discussed as two possible mechanisms for the line broadening. The measured linewidth curves show features of both mechanisms. A quantitative description of the linewidths is much more complex than for the line positions because the linewidths in both mechanisms are related to fluctuations of the coupling, whereas the line positions can be described by averaged coupling constants. The calculation of BLS linewidths in coupled magnetic trilayers remains a challenge for theory.

ACKNOWLEDGMENTS

[1] P. Grünberg, R. Schreiber, Y. Pang, M. B. Brodsky, and H. Sowers, Phys. Rev. Lett. **57**, 2442 (1986).
[2] Z. Celinski, B. Heinrich, J. F. Cochran, W. B. Muir, A. S. Arrott, and J. Kirschner, Phys. Rev. Lett. **65**, 1156 (1990).
[3] Y. Roussigné, F. Ganot, C. Dugautie, P. Moch, and D. Renard, Phys. Rev. B **52**, 350 (1995).
[4] M. J. Pechan, E. E. Fullerton, W. Robertson, M. Grimsditch, and I. K. Schuller, Phys. Rev. B **52**, 3045 (1995).
[5] A. Azevedo, C. Chesman, S. M. Rezende, F. M. de Aguiar, X. Bian, and S. S. P. Parkin, Phys. Rev. Lett. **76**, 4837 (1996).
[6] M. Grimsditch, S. Kumar, and E. E. Fullerton, Phys. Rev. B **54**, 3385 (1996).
[7] S. M. Rezende, M. A. Lucena, F. M. de Aguiar, A. Azevedo, C. Chesman, P. Kabos, and C. E. Patton, Phys. Rev. B **55**, 8071 (1997).
[8] S. M. Rezende, C. Chesman, M. A. Lucena, A. Azevedo, and F. M. de Aguiar, J. Appl. Phys. **84**, 958 (1998).
[9] P. Vavassori, M. Grimsditch, E. Fullerton, R. Zivieri, L. Giovannini, and F. Nizzoli, Surf. Sci. **454–456**, 880 (2000).
[10] P. Vavassori, M. Grimsditch, and E. E. Fullerton, J. Magn. Magn. Mater. **223**, 284 (2001).
[11] J. Barnaś and P. Grünberg, J. Magn. Magn. Mater. **82**, 186 (1989).
[12] R. R. Gareev, D. E. Bürgler, M. Buchmeier, R. Schreiber, and P. Grünberg, J. Magn. Magn. Mater. **240**, 237 (2002).
[13] B. K. Kuanr, M. Buchmeier, D. E. Bürgler, and P. Grünberg, J. Appl. Phys. **91**, 7209 (2002).
[14] M. Schäfer, S. Demokritov, S. Müller-Pfeiffer, R. Schäfer, M. Schneider, P. Grünberg, and W. Zinn, J. Appl. Phys. **77**, 6432 (1995).
[15] D. E. Bürgler, C. M. Schmidt, J. A. Wolf, T. M. Schaub, and H.-J. Güntherodt, Surf. Sci. **366**, 295 (1996).
[16] J. F. Cochran, J. Rudd, W. B. Muir, B. Heinrich, and Z. Celinski, Phys. Rev. B **42**, 508 (1990).
[17] J. F. Cochran, J. Magn. Magn. Mater. **147**, 101 (1995).
[18] M. Vohl, J. Barnaś, and P. Grünberg, Phys. Rev. B **39**, 12003 (1989).
[19] B. Hillebrands, Phys. Rev. B **41**, 530 (1990).
[20] M. Buchmeier, B. K. Kuanr, R. R. Gareev, D. E. Bügler, and P. Grünberg (unpublished).
[21] R. Coehoorn, Phys. Rev. B **44**, 9331 (1991).
[22] P. Bruno and C. Chappert, Phys. Rev. Lett. **67**, 1602 (1991).
[23] P. Bruno, Phys. Rev. B **52**, 411 (1995).
[24] N.-N. Chen, M. G. Cottam, and A. F. Khater, Phys. Rev. B **51**, 1003 (1995).
[25] J. C. Slonczewski, Phys. Rev. Lett. **67**, 3172 (1991).
[26] R. Arias and D. L. Mills, Phys. Rev. B **60**, 7395 (1999).
[27] S. M. Rezende, A. Azevedo, M. A. Lucena, and F. M. de Aguiar, Phys. Rev. B **63**, 214418 (2001).